LANGMUIR

pubs.acs.org/Langmuir Article

Spatial Segregation of Microspheres by Rubbing-Induced Triboelectrification on Patterned Surfaces

Ignaas S. M. Jimidar, Kai Sotthewes, Han Gardeniers, and Gert Desmet*

Cite This: https://dx.doi.org/10.1021/acs.langmuir.0c00959 Read Online

ACCESS | Metrics & More | Article Recommendations | Supporting Information

ABSTRACT: Particle (monolayer) assembly is essential to various scientific and industrial applications, such as the fabrication of photonic crystals, optical sensors, and surface coatings. Several methods, including rubbing, have been developed for this purpose. Here, we report on the serendipitous observation that microparticles preferentially partition onto the fluorocarbon-coated parts of patterned silicon and borosilicate glass wafers when rubbed with poly(dimethylsiloxane) slabs. To explore the extent of this effect, we varied the geometry of the pattern, the substrate material, the ambient humidity, and the material and size of the particles. Partitioning coefficients amounted up to a factor of 12 on silicon wafers and even ran in the 100s on borosilicate glass wafers at zero humidity. Using Kelvin probe force microscopy, the observations can be explained by triboelectrification, inducing a strong electrostatic attraction between the particles and the fluorocarbon zones, while the interaction with the noncoated zones is insignificant or even weakly repulsive.

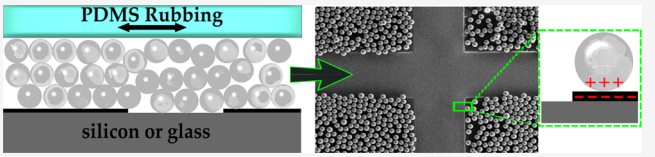

INTRODUCTION

The quest for modern miniaturized devices has driven both science and industry to study the (self-)assembly of particles into two-dimensional (2D) and three-dimensional (3D) colloidal crystals, with applications in various fields, e.g., optics, photonics, soft electronic, sensing devices, and surface coatings.[1,2] 2D spherical particle assemblies have, for example, been successfully employed as a mask in colloidal lithography for the fabrication of micro- or nanostructures.[3,4] A multifold of studies have focused on achieving self-assembled monolayers of particles dispersed in a liquid medium (wet assembly), whereas very little has been reported on the assembly under lab or dry conditions (dry assembly). Compared to the former, which relies on the evaporation rate of solvents, dry assembly is usually quick and highly effective in obtaining monolayers.[5]

One of the techniques for the assembly of particles that has been widely applied is agitation. Tien et al.[6] immersed charged gold particles and chemically patterned surfaces simultaneously in a solvent contained in a glass tube. By shaking this tube, electrostatic interactions directed the self-assembly of these particles on the patterned surfaces. Conversely, Wang et al.[7] agitated millimeter-sized nylon beads in a container and subsequently deposited these particles on a separately charged electrification layer on which the particles assemble precisely on sequentially ordered sites. Collectively, these and other studies[8−13] highlight the ability of tribocharging to direct the self-assembly of particles.

Tribocharging or contact electrification is one of the most straightforward experiments in physics and known for more than 26 centuries, yet the scientific community is still debating its underlying mechanism.[14−17] The surfaces of two solid materials, e.g., metals, semiconductors, insulators, inorganic materials, and polymers, are charged when they are brought into contact and then separated. Rubbing is particularly known to induce an electrical charge on surfaces; e.g., a balloon is charged after rubbing it on the hair of humans or animals.[17] Different charge-transfer mechanisms, such as electron transfer, ion transfer, and material transfer, have been proposed for insulators and polymers.[18−23]

Iler[24] obtained monolayers and multiple layers of particles by rubbing silica particles ranging from 50 to 200 μm on glass substrates with bare fingertips. Likewise, Dimitrov et al.[25] achieved amorphous monolayers of silica particles up to 1 μm in size by rubbing them with an oiled silicon rubber piece. Park et al.[26] rubbed 1 μm and smaller polystyrene (PS) particles between two flat poly(dimethylsiloxane) (PDMS) slabs to rapidly obtain a large-scale packed monolayer. Additionally, they painted surfaces with their dry assembled colloidal crystals to mimic color structures observed in nature.[27] Considering these and other studies,[2,5,28−31] clearly, rubbing of dry particles over surfaces is a viable method that rapidly leads to large areas covered with dry assembled colloidal crystals.

In the present study, we repeated the earlier PDMS slab-rubbing study of Park et al.,[26] but now use silicon and glass wafers coated with a patterned plasma polymer fluorocarbon

Received: April 6, 2020
Revised: May 25, 2020
Published: June 1, 2020

CF_x-layer ($2 \leq x \leq 3$).[32] The observed effect, the preferential assembly of hydrophilic silica particles on the hydrophobic CF_x-zones, is counterintuitive and has therefore been investigated in depth by changing a multitude of parameters (the pattern of the CF_x-layer, the substrate material, the humidity conditions, and the particle properties). Detailed measurements of the surface potential before and after rubbing have been conducted using Kelvin probe force microscopy (KPFM)[33] to investigate the tribocharging states in our system.[34]

RESULTS

Initial experiments were carried out using silica particles on CF_x-patterned silicon wafers at ambient conditions. Figure 1 shows a schematic representation of the generic experiment and the obtained result. Prior to rubbing, a certain amount (about 0.025 g in most experiments) of nonporous silica particles was scooped on the wafers. Rubbing typically consisted of ±10 circular manual rubbing strokes covering the entire wafer surface in a smooth circular motion (see Movie S1).

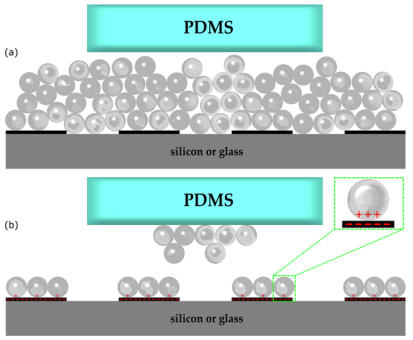

Figure 1. Schematic representation of experiment (a) before and (b) after rubbing silica particles with a PDMS slab over a silicon or glass wafer carrying a patterned CF_x-layer (indicated in black). Charges on the particles and the patterned CF_x-layer are represented by the red plus and minus signs, respectively.

Figure 2 shows that this rubbing process clearly segregates the particles according to the geometry of the patterned CF_x-layer. The CF_x-coated regions are densely occupied with a (quasi)-monolayer of particles, while only a scarce number of particles remains on the intermediate, noncoated surfaces. The nature of this particle segregation is not a priori straightforward. According to the literature,[35] hydrophilic silica particles can be expected to adhere preferentially to the hydrophilic noncoated regions, whereas here, the opposite is observed. On the other hand, the fact that the rubbing of particles against polymer surfaces produces a particle monolayer is well known from the literature.[24,26−31]

Presumably, the segregation depicted in Figure 2 is not perfect, partly due to the following steric effect: since the process preferentially leads to a monolayer, the removal of any local excess of particles will inevitably also shift particles back onto the noncoated areas, thus reducing the degree of segregation. This process is possibly enhanced by the geometrical mismatch between the pattern of the circular rubbing motion and the rectilinear pattern of the noncoated areas. The strongest segregation typically occurred when applying around 10 consecutive strokes. Fewer strokes led to incomplete segregation and more strokes led to a gradual depletion of particles as the movement of the PDMS slab also induces a net transport of particles to the rim of the wafer. In addition, as the layer of particles gets progressively more and more smeared out, even larger fractions of the particles tend to irreversibly adhere to the PDMS slab. This constitutes another important sink of particles.

As shown in Figure S1 (Supporting Information), the particles remaining on the noncoated areas can be relatively easily removed by blowing pressurized nitrogen gas at 4 bar with an air gun. This also nonspecifically removes some of the particles from the CF_x-layer, but overall, the degree of

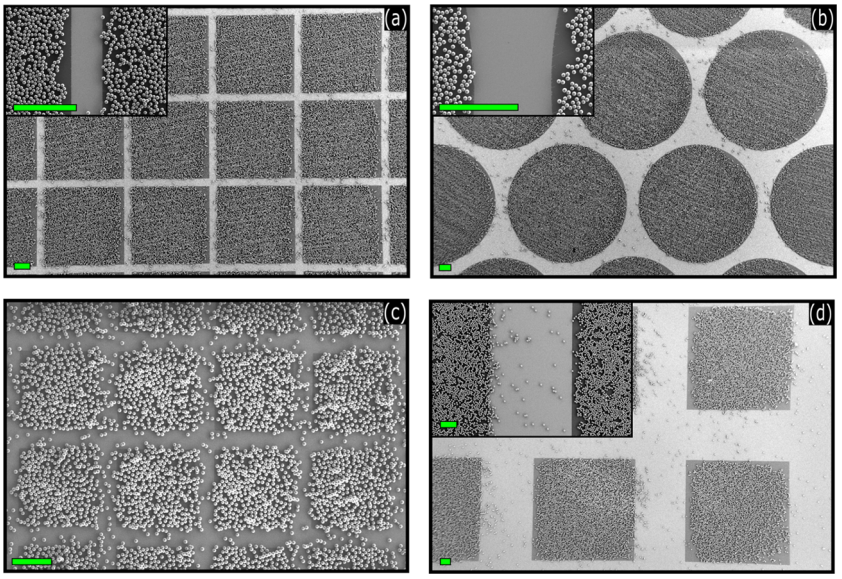

Figure 2. Scanning electron microscopy (SEM) images of the silica particle distribution after rubbing on (a) an array of CF_x-squares (500 μm × 500 μm; spacing = 50 μm), (b) an array of CF_x-circles with a diameter of 1 mm and a spacing of 50 μm, (c) an array of CF_x-squares (200 μm × 200 μm; spacing = 50 μm), and (d) an array of CF_x-squares (1 mm × 1 mm; spacing = 500 μm). Scale bar in all images is 100 μm. Particle size: 5 μm in (a, b) and 10 μm in (c, d). Conditions: ambient humidity, silicon wafer.

https://dx.doi.org/10.1021/acs.langmuir.0c00959
Langmuir XXXX, XXX, XXX−XXX

segregation is clearly enhanced, cf. the increase of the partitioning coefficient P from P = 7.5 to 28 for the example shown in Figure S1 (definition of P in eq 1 further on). This suggests the occurrence of a strong adhesion force between the particles and the CF_x-coated areas, while the presence of the few remaining particles on the noncoated surfaces is clearly more of an accidental nature. This strong adhesion force is nevertheless weaker than the adhesion force that can be exerted by pushing a new, unused PDMS slab against the formed segregation pattern. As shown in Figure S2 of the Supporting Information, this action allows us to remove most of the adhered particles and transfer the assembled pattern in a nearly perfectly intact way onto the new slab.

The magnitude of the segregation effect has been investigated over a wide range of the size, shape, and spacing of the CF_x-coated surface zones. Figure 3 gives an overview of

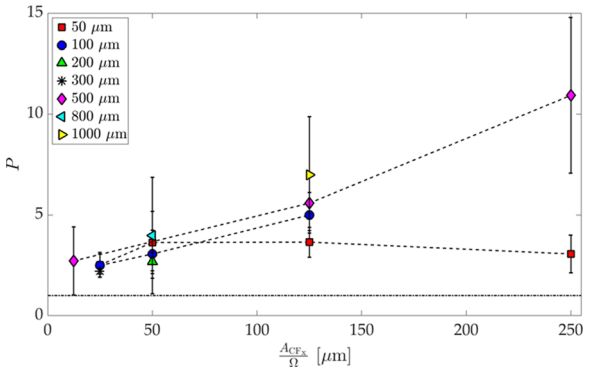

Figure 3. Partitioning coefficient P as a function of the area A_{CF_x} over the perimeter Ω ratio of the CF_x-coated regions (different data point symbols relate to different spacings between adjacent squares). Error bars represent the standard deviation for N = 3. Conditions: 10 μm silica particles, silicon wafers, ambient humidity. Horizontal dash-pointed line represents P = 1. Dashed lines are added to guide the eye.

the results as a function of the most important geometrical parameters. Data are presented for the square pattern case only, but very similar results were obtained with the circular CF_x-patterns. The degree of segregation is quantified using the partitioning coefficient P:

$$P = \frac{\sigma_{CF_x}}{\sigma_{Si}} \quad (1)$$

wherein P represents the ratio of the particle surface concentration σ on the coated over the noncoated areas as measured at the end of the rubbing process. To measure the particle surface concentration on the noncoated areas, a region with the width of one particle aside of the boundary between the noncoated and coated zones has been excluded to obtain the purest possible measurement of P, devoid of most of the boundary effects. These boundary effects relate to particles accidentally spilling over from the CF_x-coated zones while still being clearly linked to the layer covering the latter.

The best correlation between P and the complexity of the geometrical parameters was found with the ratio of the area A_{CF_x} of the CF_x-coated regions over their perimeter Ω. Although caution is needed given the limited number of experimental data points upon which it is based, Figure 3 shows that, provided the distance between the CF_x-coated zones is large enough (i.e., is at least 100 μm), P increases nearly linearly with this ratio. Larger coated zones have a relatively larger area A_{CF_x} compared to the perimeter Ω. Therefore, more particles can be contained in a larger area, while fewer particles can spill over the boundary of the coated zones, thus increasing the P-value. When the distance between the CF_x-squares is only 50 μm (red squares) or less (data not shown), partitioning coefficients remain low ($P \leq 2-3$), regardless of the size of the CF_x-zones. This appears to be in line with the fact that, when the interspacing becomes too small, the noncoated areas are relatively much more rapidly filled with particles coming in a nonselective way from the CF_x-zones (note that the 50 μm interzone distance is only 5 particles wide in the present 10 μm particle case). Comparing the P-values for the same CF_x-zone size (i.e., comparing the data points in Figure 3 in the vertical direction) further emphasizes the importance of the distance between the noncoated zones, as the achievable P clearly increases with the interspacing.

Within the investigated range, there was no significant effect of the particle size on the value of P. Comparing the partitioning coefficient P for 5 vs 10 μm silica particles for the same CF_x-pattern consistently yielded P-values that deviated less than 1 standard deviation; e.g., for two designs with an equal spacing of 50 μm, the P-value = 2.6 vs 3.6 (200 μm × 200 μm) and the P-value = 4 vs 3.6 (500 μm × 500 μm). Obviously, it is difficult to predict how the P-values would vary if stronger conditions in particle size would be considered. Experiments involving much larger (e.g., 50 μm) or much smaller (e.g., 500 nm) particles would be needed for this.

To investigate one of our research hypotheses (silica particles lose their charge acquired above the CF_x-coated

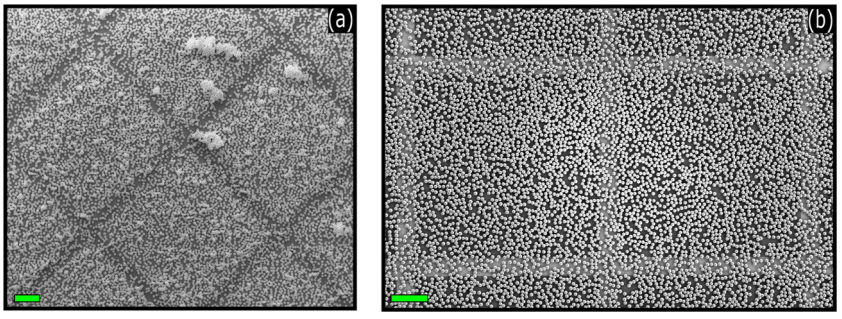

Figure 4. SEM images of the particle distribution after rubbing 10 μm silica particles over an array of CF_x-squares (500 μm × 500 μm; spacing = 50 μm) (a) using the HF-etched silicon wafer (rubbing carried out under ambient humidity) conditions and (b) using a regular, non-HF-etched silicon wafer inside a glove box at zero humidity. Scale bar in both images is 100 μm.

https://dx.doi.org/10.1021/acs.langmuir.0c00959
Langmuir XXXX, XXX, XXX−XXX

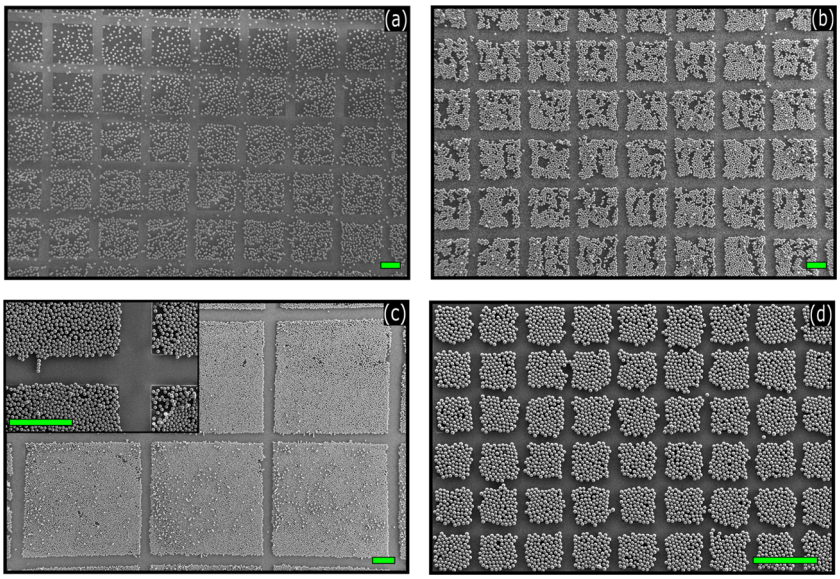

Figure 5. SEM images of the particle distribution after rubbing silica particles over the patterned borosilicate glass wafers covered with an array of CF_x-squares. (a, b) Particle size = 10 μm; 200 μm × 200 μm squares; spacing = 50 μm (a) under ambient conditions and (b) inside a glovebox at zero humidity. (c, d) Experiments performed with 5 μm silica particles inside the glovebox using (c) 500 μm × 500 μm CF_x-squares; spacing = 50 μm; and (d) 50 μm × 50 μm CF_x-squares; spacing = 20 μm. Scale bar in all images is 100 μm.

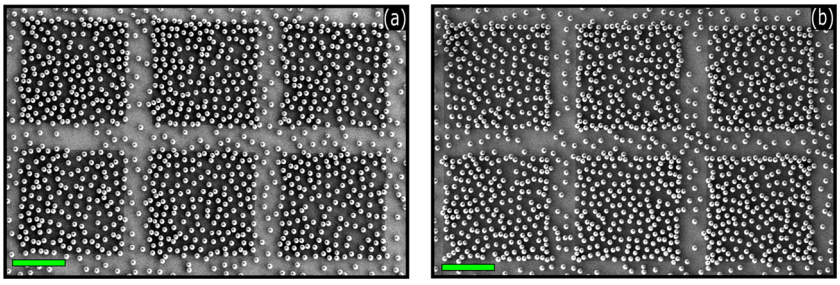

Figure 6. SEM images of the particle distribution after rubbing 10 μm hydrophobic PS particles over an array of CF_x-squares (200 μm × 200 μm; spacing = 50 μm) arranged on a silicon wafer (a) under ambient conditions and (b) inside a glovebox at zero humidity. Scale bar in both images is 100 μm.

zones when dragged again onto the intermediate noncoated surfaces), the initial experiments were repeated with wafers carrying thermally grown silicon oxide layers in an attempt to suppress or even block the presumed discharge process. The results shown in Figure S3a−c of the Supporting Information clearly show that an increase in the thickness of the insulating layer does not affect the segregation process at all. The segregation process even proceeds with at least the same intensity when using borosilicate glass wafers (Figure S3d), even though these have a conductivity that is at least 8 orders of magnitude smaller than the silicon wafers. Experiments were also conducted with silicon wafers after removal of the native oxide layer by wet hydrofluoric acid (HF)-etching. Subsequently, the rubbing experiments were performed within 15 min after this etching.[36] As can be noted from Figure 4a, the segregation is now significantly weaker, P = 1.9 vs 3.6, when the native oxide layer is present (data for the same geometry, 500 μm × 500 μm, 50 μm interspacing).

To verify the contribution of the ambient humidity, experiments were also performed inside a glovebox (<0.5 ppm H_2O molecules). Figure 4b shows that the segregation, in this case, is also much weaker, if not insignificant (P = 1.1 vs 3.6 outside the glovebox; data for the same geometry as above), implying that humidity is a crucial factor in the segregation process of silica particles on the silicon wafers. On the other hand, the low humidity conditions do not impede the segregation effect on the borosilicate glass wafers (Figure 5). Even more, the segregation on the glass wafers was consistently found to be more pronounced inside the glovebox than under ambient conditions (e.g., compare Figure 5b with 55a). The combination of borosilicate glass wafers with the quasi-zero humidity conditions in the glovebox in fact produced the highest observed degree of segregation in the present study (P = 220 in Figure 5c). The segregation on borosilicate glass wafers in the glovebox even proceeds to the extent that a 20 μm distance between the coated zones is sufficient to achieve P-values as high as 30 (Figure 5d), whereas this spacing was much too small to lead to significant segregation on silicon wafers.

To investigate the influence of the hydrophobic/hydrophilic nature of the particles, the rubbing experiments were also repeated with 10 μm hydrophobic polystyrene (PS) particles. Figure 6 shows that also the PS particles preferentially assemble on the CF_x-surfaces but achieve a packing density that is much lower than with the silica particles as the individual PS particles clearly repel each other. This inevitably limits the available space for the particles on the CF_x-surfaces, explaining the lower observed partitioning coefficients (e.g., P

https://dx.doi.org/10.1021/acs.langmuir.0c00959
Langmuir XXXX, XXX, XXX−XXX

= 2.5 and 2.3 for PS particle cases in Figure 6 vs P = 3.6 for silica particles on the same 200 μm × 200 μm geometry outside the glovebox). Interestingly, and in contrast with the silica particles, there was no significant difference between the segregation of the PS particles inside and outside of the glovebox.

To understand the origin of the above observations, Kelvin probe force microscopy (KPFM) measurements (Figure S4) were conducted to measure the surface contact potential difference on the different wafer surfaces and the particles. Interpreting the results shown in Figure 7, it should be kept in mind that the sign of the V_{CPD}-values is always the opposite of the sign of the surface charge (see Section S3b). Unfortunately, KPFM-measurements were only possible under ambient humidity and not under dry air conditions.

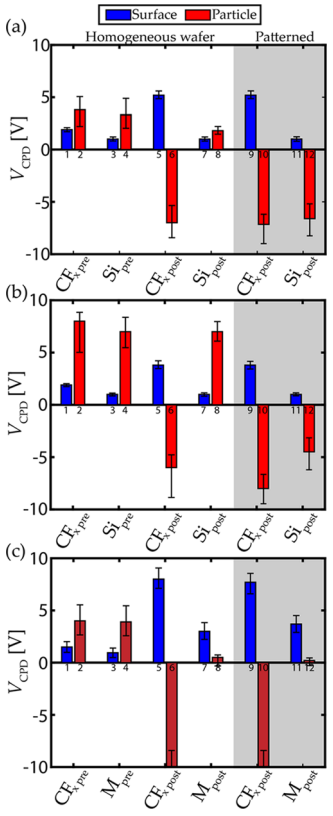

Figure 7. Histograms of the contact potential difference (V_{CPD}) measured on the fluorocarbon-coated (CF_x) and noncoated silicon (Si) and borosilicate glass (M) surfaces (blue) and on the particles (red) before (pre) and after (post) rubbing for (a) 5 μm silica particles on a uniform CF_x-coated and noncoated wafer, as well as a patterned silicon wafer; (b) 3 μm polystyrene particles on a uniform CF_x-coated and noncoated wafer, as well as a patterned silicon wafer; and for (c) 5 μm silica particles on a uniform CF_x-coated and noncoated wafer, as well as a patterned borosilicate glass wafer. Numbers 1−12 are used for referencing in the text; numbers 1−8 relate to uniformly coated or noncoated wafers (1−4: before rubbing, 5−8 after rubbing); and numbers 9−12 (gray-shaded area) relate to patterned wafers after rubbing. Error bars represent the minimum and the maximum measured values (N > 4 for the results in (a, b) and N > 2 for the results in (c)).

A first important observation was that no significant effect of the CF_x-zone size on the measured surface potentials was observed (see the error bars on data in Figure 7, assembled across a mix of coated zone sizes). The data for silica on silicon (Figure 7a) show that rubbing silica particles against the CF_x-coating charges the CF_x-surface negatively (V_{CPD}-value of bar #5 has become more positive compared to the initial surface state represented by bar #1), while the silica particles clearly obtain a positive charge (compare bar #6 with bar #2). This agrees with the position of both materials in the triboseries and indicates a strong electrostatic attraction between the particles and the CF_x-surface. Bar #5 and bar #9 have a similar height, as is the case for bar #6 and bar #10, showing that this charging process proceeds to the same extent regardless of whether the CF_x-surface is interrupted by noncoated silicon wafer zones. Figure 7a also shows that the rubbing does not have a significant effect on the charge of the silicon wafer surface (compare bar #3 with bar #7), while the silica particles even tend to lose a bit of their charge by rubbing (compare bar #4 with bar #8).

The V_{CPD}-values reported on the silica particles found on the noncoated zones of the patterned wafers after rubbing (bar #12) need to be interpreted with care, for these were obviously measured on particles that still adhered to the silicon surface after the rubbing process, while the vast majority of the silica particles has been removed from this surface and hence might have had another (smaller) potential and charge, as they could not withstand the rubbing action. Considering furthermore that the particle charge measured when rubbing the particles against a uniform, noncoated silicon wafer (bar #8) is much more likely to represent the intrinsic particle charge state above the noncoated zones, it can be inferred that the large potential represented by bar #12 relates to particles that have acquired their charge while being rubbed against the CF_x-coating (see also the similarity between bar #12 with bars #6 and #10) and did not have had the opportunity yet to discharge.

The KPFM-measurements were also repeated for the PS particles (Figure 7b). The main difference with the silica particle case is that the PS particles already carry a relatively strong (negative) charge in their initial state (cf. bars #2 and #4 in Figure 7b). This charge obviously is reversed when rubbed against a CF_x-surface (bar #6 has a sign that is opposite to those of bars #2 and #4). At the same time, the CF_x-surface also acquires a larger (negative) charge (compare bar #5 with bar #1). The opposite charges acquired by the CF_x-surface and the PS particles is in agreement with their mutual position in the triboseries for polymers.[37] The charge on the PS particles, on the other hand, remains unaltered when rubbed against a silicon wafer surface (bar #8 is very similar to bars #2 and #4). The same applies to the charge of the silicon wafer surface.

Figure 7c summarizes the KPFM-measurements for silica particles on borosilicate glass wafers, showing that the surface potential on both the silica particles and the CF_x-surfaces is significantly larger than on the silicon wafer (compare Figure 7a and 77c for bar #5 and bar #6). This signifies that the charge is not only determined by the material of the top layer (CF_x in both cases) but also by the underlying substrate material (silicon vs borosilicate glass). This finding is in agreement with a study reported by Siek et al.[38] Note that the potential on the particles even exceeded the lower measurement limit of the instrument (bars #6 and #10 are fully saturated).

As in the silicon wafer case, the charge on the particles adhered to the CF_x-surfaces on the patterned borosilicate glass wafer is very similar to that on a uniformly CF_x-coated glass wafer (cf. bars #6 and #10 in Figure 7c). The surface potential of the particles on the pure borosilicate glass wafer (bar #8), as

https://dx.doi.org/10.1021/acs.langmuir.0c00959
Langmuir XXXX, XXX, XXX−XXX

well as on the noncoated parts of the patterned wafer (bar #12), is in both cases very small. This is a clear difference with the silicon wafer case in Figure 7a.

DISCUSSION

To rationalize the observed effects, hydrophilic/hydrophilic attraction effects based on capillary forces[35] can be discarded because in this case, the hydrophilic silica particles would adhere preferentially to the hydrophilic noncoated silicon or borosilicate glass wafer surfaces and not to the hydrophobic CF_x-coated zones, as is consistently observed here.

On the other hand, the observations made for the silica particles are consistent with a mechanism wherein, given their position in the triboelectric series, the silica particles acquire a large positive charge by triboelectrification when rubbed against the CF_x-surfaces, which in turn acquire a large negative charge (Figure 1b). Due to these opposite charges, a strong electrostatic attraction force establishes between the silica particles and the CF_x-surfaces. The CF_x layer is characterized in the literature[37] as the most negatively charged polymer in the triboseries, thus enhancing the segregation effect. The noncoated wafer surfaces on the other hand either do not significantly charge (silicon wafers) or acquire a negative charge, which, combined with the small negative charge on the silica particles, even leads to a repulsive electrostatic force (borosilicate glass wafers), albeit a weak one (at least under ambient humidity).

The net result of the above is that the mechanical force exerted by the rubbing surface can much more easily transport particles across the noncoated wafer surfaces than across the CF_x-surfaces, where they are withheld by a strong electrostatic attraction, thus explaining the observed segregation effect.

Considering that the KPFM-measurements were found to be independent of the size of the coated zones while the partitioning coefficient P clearly varies with the coated zone sizes (Figure 3), the measured P-values must also be influenced by an important geometrical effect. Larger coated zones have a relatively larger area compared to the circumference Ω along which particles can spill over to the noncoated areas under the influence of the mechanical rubbing process, hence explaining the inversely proportional relation of the P-value with Ω in Figure 3. The opposite holds for the effect of the area of the coated zones: the larger this area, the smaller the probability that particles come close to the zone boundary where they can be swept onto the noncoated zones by the rubbing motion. This geometric effect is more pronounced on silicon wafers than on glass wafers. This is in turn most probably a consequence of the stronger electrostatic forces exerted on the patterned glass wafers, leaving less room to the nonselective action of the rubbing motion.

Since the segregation of silica particles on patterned silicon wafers is significantly weaker than under zero humidity conditions (P = 3.6 under ambient humidity vs P = 1.1 within the glovebox), we also postulate that the segregation process is in this case enhanced by a local discharging process experienced by the silica particles when moving from the CF_x-surfaces onto the noncoated silicon wafer surfaces. This could be explained by the fact that, under ambient conditions, water vapor inevitably condensates into a thin surface layer on the hydrophilic noncoated silicon wafer parts, thus allowing the formation of a capillary bridge between the silica particles and the silicon wafer surface through which the particles can discharge, following a mechanism already described by Pence et al.[39] Contrary to one's intuition, higher humidity levels might not de facto enhance the degree of segregation. Tribocharged surfaces contain less charge due to higher surface conductivity, reducing the electrostatic interactions.[39−41] Particle discharge by conductance through the wafer can be discarded given the undiminished persistence of the particle segregation effect on substrates with a reduced electrical conductivity (thermally oxidized Si-wafers, borosilicate glass wafers).

The contribution of an adsorbed water layer is also consistent with the fact that the particle segregation is clearly weaker when the native SiO_2-layer covering the silicon surface was removed (P = 3.6 with the native layer present vs P = 1.9 with the layer removed). HF-etching renders the silicon surface more hydrophobic, therewith reducing the presence of a bound water monolayer,[42] which in turn lowers the silica particles' opportunity to discharge.

The stronger segregation effect on the borosilicate glass wafers can be attributed to the stronger induced electrostatic attraction between the silica particles and the CF_x-surfaces, in turn resulting from the fact that both the CF_x-surfaces and the silica particles acquire a larger (opposite) charge on borosilicate glass surfaces than on silicon surfaces. The stronger segregation is also consistent with the significantly higher hydrophilicity of borosilicate glass vs silicon (contact angle 10 vs 35°, cf. Table S1), thus providing an enhanced opportunity for local particle discharge via a bound water layer. This might also explain the very low charges measured on the (few) particles found on the noncoated borosilicate glass wafer areas.

The observation that the segregation process on the borosilicate glass wafers also occurs within the glovebox, whereas this is not the case for the silicon wafers, is more difficult to explain given the lack of KPFM-measurements under glovebox conditions. At present, we can therefore only speculate that this is due to the fact that the electrostatic forces (attractive above the CF_x-coated zones and repulsive above the noncoated zones) are even more pronounced at zero humidity, as it can be expected that the charge decay will be weaker under these conditions.[38,41,43] The fact that the silica particles can assemble in a very close packing on the CF_x-coated zones on both the silicon and especially on the borosilicate glass wafers implies that they do not exhibit any significant mutual repulsion, despite the particles carrying the same charge sign. It is assumed that this is because the electrostatic force attracting the particles to the CF_x-coated zones outweighs the mutual repulsion forces between the particles. Another contributing factor might be, as described in the literature for charged dielectric particles,[44,45] that the dielectrophoretic force induced by the polarization between silica particles is larger than the mutual Coulomb repulsion, resulting in an attractive electrostatic force between the particles.

The segregation observed for the hydrophobic polystyrene (PS) particles can be explained using the same tribocharging mechanism as described for the silica particles, given that the trend of the KPFM-measurement is very similar (cf. Figure 7a,b). The most striking difference, however, is the clear mutual repulsion of the individual PS particles, as opposed to the dense packing formed by the silica particles. A potential explanation for this mutual repulsion is that in contrast to the silica particles, the polarization-induced dielectrophoretic force does not lead to an electrostatic attraction between the PS particles. This is justified since the permittivity of PS is at least

https://dx.doi.org/10.1021/acs.langmuir.0c00959
Langmuir XXXX, XXX, XXX−XXX

2× smaller than that of silica, resulting in less polarization and mutual electrostatic attraction.[46] The fact that the humidity conditions have a much smaller effect on the segregation for PS particles than with silica particles can be attributed to the hydrophobic nature of the PS particles.[41]

Apart from the equilibrium between the electrostatic and mechanic forces and the charging and discharging processes, the observed *P*-values are certainly also influenced by the motion pattern of the manual rubbing process, as well as by the amount and initial distribution of the particles. Both factors were poorly controlled in the present study, given the manual nature of the employed procedures. Possibly, the reproducibility and quality of the segregation effect could be enhanced by moving to automated and motorized processes to obtain better control over the pressure and motion of the rubbing process and the initial distribution of the particles.

CONCLUSIONS

Silica and polystyrene (PS) particles rubbed with a PDMS slab past silicon and borosilicate glass wafers carrying a patterned fluorocarbon (CF_x) coating strongly segregate and self-organize in quasi-monolayers, matching the geometrical pattern of the coated zones (e.g., cubic grid of squares or equilateral triangular grid of circles), despite the circular pattern of the rubbing motion. Partitioning coefficients up to $P = 12$ were measured on patterned silicon wafers, while *P*-factors on patterned borosilicate glass wafers can even easily run in the 100s. These numbers were found to be independent of the investigated particle size (5 and 10 μm), but for further research, a broader range of particle sizes is preferable to determine the limit of the segregation effect. KPFM-measurements support the hypothesis that the segregation is induced by tribocharging of the particles and the CF_x-coated zones, acquiring opposite charges and thus inducing a strong electrostatic attraction force between the CF_x-surfaces and the particles. On the noncoated zones, on the other hand, there is either no significant tribocharging (silicon wafers) or even a repulsive tribocharging (borosilicate glass wafers), such that the rubbing motion can induce a net transport of particles from the noncoated to the coated zones.

For silica particles on silicon wafers, the process appears to be critically supported by the presence of air moisture stimulating the particles to discharge when moving from the CF_x-coated zones to the noncoated zones. On borosilicate glass wafers, both the silica particles and the CF_x-coated zones charge more strongly. This might render the presence of air moisture less critical.

The segregation effect is also observed when using hydrophobic PS particles instead of hydrophilic silica particles, albeit that in this case, the segregation is not as pronounced (*P*-factors on the order of 2.5) and that the particles do not assemble in a dense packing but appear as isolated individual particles.

Despite its exploratory nature and limitations, the present study provides a rapid method to electrostatically self-assemble closely packed silica particles on patterned borosilicate glass wafer surfaces (segregation on silicon wafers is not perfect). A drawback is that the method only works well, provided that the number of particles is sufficiently high to cover the entire wafer with a quasi-monolayer. If the number of particles drops below this critical level, the movement of the PDMS slab is no longer sufficiently lubricated. The existence of a lower limit on the number of particles implies that the process is inevitably carried out in a regime that is close to an overload of the monolayer saturation capacity of the CF_x-coated zones. This in turn creates a situation wherein the realized partitioning coefficients are inevitably affected by the interplay between the geometrical pattern and the rubbing motion, causing excess particles to spill over from the coated onto the noncoated zones.

ASSOCIATED CONTENT

Supporting Information

The Supporting Information is available free of charge at https://pubs.acs.org/doi/10.1021/acs.langmuir.0c00959.

Experimental details, patterning of substrates, methods, results, additional data, table, and figures (PDF)

Circular manual rubbing strokes covering the entire wafer surface in a smooth circular motion (MP4)

AUTHOR INFORMATION

Corresponding Author

Gert Desmet − *Department of Chemical Engineering CHIS, Vrije Universiteit Brussel, Brussels 1050, Belgium*; Email: gedesmet@vub.be

Authors

Ignaas S. M. Jimidar − *Department of Chemical Engineering CHIS, Vrije Universiteit Brussel, Brussels 1050, Belgium; Mesoscale Chemical Systems, University of Twente, Enschede 7522 NB, The Netherlands;* orcid.org/0000-0001-9653-1938

Kai Sotthewes − *Physics of Interfaces and Nanomaterials, University of Twente, Enschede 7522 NB, The Netherlands;* orcid.org/0000-0003-2073-6958

Han Gardeniers − *Mesoscale Chemical Systems, University of Twente, Enschede 7522 NB, The Netherlands;* orcid.org/0000-0003-0581-2668

Complete contact information is available at: https://pubs.acs.org/10.1021/acs.langmuir.0c00959

Notes

The authors declare no competing financial interest.

ACKNOWLEDGMENTS

The authors gratefully acknowledge funding from the ERC Advanced Grant "PrintPack" (No. 695067).

REFERENCES

(1) Vogel, N.; Retsch, M.; Fustin, C.-A.; del Campo, A.; Jonas, U. Advances in colloidal assembly: the design of structure and hierarchy in two and three dimensions. *Chem. Rev.* **2015**, *115*, 6265−6311.

(2) Hwang, H.; Jeong, U. Microparticle-Based Soft Electronic Devices: Toward One-Particle/One-Pixel. *Adv. Funct. Mater.* **2020**, *30*, No. 1901810.

(3) Liang, X.; Dong, R.; Ho, J. C. Self-Assembly of Colloidal Spheres toward Fabrication of Hierarchical and Periodic Nanostructures for Technological Applications. *Adv. Mater. Technol.* **2019**, *4*, No. 1800541.

(4) Zhang, X. A.; Chen, I.-T.; Chang, C.-H. Recent progress in near-field nanolithography using light interactions with colloidal particles: from nanospheres to three-dimensional nanostructures. *Nanotechnology* **2019**, *30*, No. 352002.

(5) Khanh, N. N.; Yoon, K. B. Facile organization of colloidal particles into large, perfect one-and two-dimensional arrays by dry manual assembly on patterned substrates. *J. Am. Chem. Soc.* **2009**, *131*, 14228−14230.

(6) Tien, J.; Terfort, A.; Whitesides, G. M. Microfabrication through electrostatic self-assembly. *Langmuir* **1997**, *13*, 5349−5355.
(7) Wang, Y.; Wei, X. Y.; Kuang, S. Y.; Li, H. Y.; Chen, Y. H.; Liang, F.; Su, L.; Wang, Z. L.; Zhu, G. Triboelectrification-Induced Self-Assembly of Macro-Sized Polymer Beads on a Nanostructured Surface for Self-Powered Patterning. *ACS Nano* **2018**, *12*, 441−447.
(8) Cezan, S. D.; Nalbant, A. A.; Buyuktemiz, M.; Dede, Y.; Baytekin, H. T.; Baytekin, B. Control of triboelectric charges on common polymers by photoexcitation of organic dyes. *Nat. Commun.* **2019**, *10*, No. 276.
(9) Cademartiri, R.; Stan, C. A.; Tran, V. M.; Wu, E.; Friar, L.; Vulis, D.; Clark, L. W.; Tricard, S.; Whitesides, G. M. A simple two-dimensional model system to study electrostatic-self-assembly. *Soft Matter* **2012**, *8*, 9771−9791.
(10) Liu, Y.; Wang, A.; Claus, R. O. Layer-by-layer electrostatic self-assembly of nanoscale Fe 3 O 4 particles and polyimide precursor on silicon and silica surfaces. *Appl. Phys. Lett.* **1997**, *71*, 2265−2267.
(11) McCarty, L. S.; Winkleman, A.; Whitesides, G. M. Electrostatic self-assembly of polystyrene microspheres by using chemically directed contact electrification. *Angew. Chem., Int. Ed.* **2007**, *46*, 206−209.
(12) Winkleman, A.; Gates, B. D.; McCarty, L. S.; Whitesides, G. M. Directed self-assembly of spherical particles on patterned electrodes by an applied electric field. *Adv. Mater.* **2005**, *17*, 1507−1511.
(13) Grzybowski, B. A.; Winkleman, A.; Wiles, J. A.; Brumer, Y.; Whitesides, G. M. Electrostatic self-assembly of macroscopic crystals using contact electrification. *Nat. Mater.* **2003**, *2*, 241.
(14) Liu, C.; Bard, A. J. Electrostatic electrochemistry at insulators. *Nat. Mater.* **2008**, *7*, 505.
(15) Xu, C.; Zi, Y.; Wang, A. C.; Zou, H.; Dai, Y.; He, X.; Wang, P.; Wang, Y.-C.; Feng, P.; Li, D.; Wang, Z. L. On the Electron-Transfer Mechanism in the Contact-Electrification Effect. *Adv. Mater.* **2018**, *30*, No. 1706790.
(16) Pan, S.; Zhang, Z. Fundamental theories and basic principles of triboelectric effect: A review. *Friction* **2019**, *7*, 2−17.
(17) Lacks, D. J.; Shinbrot, T. Long-standing and unresolved issues in triboelectric charging. *Nat. Rev. Chem.* **2019**, *3*, 465−476.
(18) Diaz, A. F.; Felix-Navarro, R. M. A semi-quantitative tribo-electric series for polymeric materials: the influence of chemical structure and properties. *J. Electrost.* **2004**, *62*, 277−290.
(19) McCarty, L. S.; Whitesides, G. M. Electrostatic charging due to separation of ions at interfaces: contact electrification of ionic electrets. *Angew. Chem., Int. Ed.* **2008**, *47*, 2188−2207.
(20) Lacks, D. J.; Sankaran, R. M. Contact electrification of insulating materials. *J. Phys. D: Appl. Phys.* **2011**, *44*, No. 453001.
(21) Baytekin, H. T.; Baytekin, B.; Incorvati, J. T.; Grzybowski, B. A. Material transfer and polarity reversal in contact charging. *Angew. Chem., Int. Ed.* **2012**, *51*, 4843−4847.
(22) Galembeck, F.; Burgo, T. A. L.; Balestrin, L. B. S.; Gouveia, R. F.; Silva, C. A.; Galembeck, A. Friction, tribochemistry and triboelectricity: recent progress and perspectives. *RSC Adv.* **2014**, *4*, 64280−64298.
(23) Chen, L.; Shi, Q.; Sun, Y.; Nguyen, T.; Lee, C.; Soh, S. Controlling Surface Charge Generated by Contact Electrification: Strategies and Applications. *Adv. Mater.* **2018**, *30*, No. 1802405.
(24) Iler, R. K. The adhesion of submicron silica particles on glass. *J. Colloid Interface Sci.* **1972**, *38*, 496−501.
(25) Dimitrov, A. S.; Miwa, T.; Nagayama, K. A comparison between the optical properties of amorphous and crystalline monolayers of silica particles. *Langmuir* **1999**, *15*, 5257−5264.
(26) Park, C.; Lee, T.; Xia, Y.; Shin, T. J.; Myoung, J.; Jeong, U. Quick, Large-Area Assembly of a Single-Crystal Monolayer of Spherical Particles by Unidirectional Rubbing. *Adv. Mater.* **2014**, *26*, 4633−4638.
(27) Park, C.; Koh, K.; Jeong, U. Structural color painting by rubbing particle powder. *Sci. Rep.* **2015**, *5*, No. 8340.
(28) Koh, K.; Hwang, H.; Park, C.; Lee, J. Y.; Jeon, T. Y.; Kim, S.-H.; Kim, J. K.; Jeong, U. Large-Area Accurate Position Registry of Microparticles on Flexible, Stretchable Substrates Using Elastomer Templates. *ACS Appl. Mater. Interfaces* **2016**, *8*, 28149−28158.
(29) Hwang, H.; Choi, S.-E.; Han, S. W.; You, I.; Jeong, E. S.; Kim, S.; Yang, H.; Lee, S.; Choo, J.; Kim, J. W.; et al. Cut-and-Paste Transferrable Pressure Sensing Cartridge Films. *Chem. Mater.* **2018**, *30*, 6410−6419.
(30) You, I.; Choi, S.-E.; Hwang, H.; Han, S. W.; Kim, J. W.; Jeong, U. E-Skin Tactile Sensor Matrix Pixelated by Position-Registered Conductive Microparticles Creating Pressure-Sensitive Selectors. *Adv. Funct. Mater.* **2018**, *28*, No. 1801858.
(31) Kang, K.; Choi, S.-E.; Jang, H. S.; Cho, W. K.; Nam, Y.; Choi, I. S.; Lee, J. S. In vitro developmental acceleration of hippocampal neurons on nanostructures of self-assembled silica beads in filopodium-size ranges. *Angew. Chem., Int. Ed.* **2012**, *51*, 2855−2858.
(32) Jansen, H. V.; Gardeniers, J. G. E.; Elders, J.; Tilmans, H. A. C.; Elwenspoek, M. Applications of fluorocarbon polymers in micro-mechanics and micromachining. *Sens. Actuators, A* **1994**, *41*, 136−140.
(33) Melitz, W.; Shen, J.; Kummel, A. C.; Lee, S. Kelvin probe force microscopy and its application. *Surf. Sci. Rep.* **2011**, *66*, 1−27.
(34) Wang, Z. L.; Wang, A. C. On the origin of contact-electrification. *Mater. Today* **2019**, *30*, 34−51.
(35) Jones, R.; Pollock, H. M.; Cleaver, J. A.; Hodges, C. S. Adhesion forces between glass and silicon surfaces in air studied by AFM: Effects of relative humidity, particle size, roughness, and surface treatment. *Langmuir* **2002**, *18*, 8045−8055.
(36) Miura, T.-a.; Niwano, M.; Shoji, D.; Miyamoto, N. Kinetics of oxidation on hydrogen-terminated Si (100) and (111) surfaces stored in air. *J. Appl. Phys.* **1996**, *79*, 4373−4380.
(37) Zhang, X.; Chen, L.; Jiang, Y.; Lim, W.; Soh, S. Rationalizing the Triboelectric Series of Polymers. *Chem. Mater.* **2019**, *31*, 1473−1478.
(38) Siek, M.; Adamkiewicz, W.; Sobolev, Y. I.; Grzybowski, B. A. The influence of distant substrates on the outcome of contact electrification. *Angew. Chem., Int. Ed.* **2018**, *57*, 15379−15383.
(39) Pence, S.; Novotny, V. J.; Diaz, A. F. Effect of surface moisture on contact charge of polymers containing ions. *Langmuir* **1994**, *10*, 592−596.
(40) Németh, E.; Albrecht, V.; Schubert, G.; Simon, F. Polymer tribo-electric charging: dependence on thermodynamic surface properties and relative humidity. *J. Electrost.* **2003**, *58*, 3−16.
(41) Schella, A.; Herminghaus, S.; Schröter, M. Influence of humidity on tribo-electric charging and segregation in shaken granular media. *Soft Matter* **2017**, *13*, 394−401.
(42) Chen, L.; He, X.; Liu, H.; Qian, L.; Kim, S. H. Water adsorption on hydrophilic and hydrophobic surfaces of silicon. *J. Phys. Chem. C* **2018**, *122*, 11385−11391.
(43) Baytekin, H. T.; Baytekin, B.; Soh, S.; Grzybowski, B. A. Is water necessary for contact electrification. *Angew. Chem., Int. Ed.* **2011**, *50*, 6766−6770.
(44) Feng, J. Q. Electrostatic interaction between two charged dielectric spheres in contact. *Phys. Rev. E* **2000**, *62*, 2891−2897.
(45) Matias, A. F. V.; Shinbrot, T.; Araújo, N. A. M. Mechanical equilibrium of aggregates of dielectric spheres. *Phys. Rev. E* **2018**, *98*, No. 062903.
(46) Bichoutskaia, E.; Boatwright, A. L.; Khachatourian, A.; Stace, A. J. Electrostatic analysis of the interactions between charged particles of dielectric materials. *J. Chem. Phys.* **2010**, *133*, No. 024105.

https://dx.doi.org/10.1021/acs.langmuir.0c00959
Langmuir XXXX, XXX, XXX−XXX